American Mineralogist, Volume 92, pages 370–379, 2007

Effect of variable carbonate concentration on the solidus of mantle peridotite

RAJDEEP DASGUPTA* AND MARC M. HIRSCHMANN

Department of Geology and Geophysics, University of Minnesota, 310 Pillsbury Drive SE, Minneapolis, Minnesota 55455, U.S.A.

ABSTRACT

To explore the effect of variable CO_2 concentrations on the solidus of natural carbonated peridotite, we determined near-solidus phase relations of three different nominally anhydrous, carbonated lherzolite bulk compositions at 6.6 GPa. Starting mixes (PERC, PERC2, and PERC3) were prepared by adding variable proportions of a carbonate mixture that has the same Ca:Mg:Fe:Na:K ratio as the base silicate peridotite [MixKLB-1: Mg no. = 89.7; Ca no. = molar Ca/(Ca + Mg + Fe*) = 0.05]. For all three bulk compositions, the subsolidus assemblage includes olivine, orthopyroxene, clinopyroxene, garnet, and magnesite solid solutions. Above the solidus, crystalline carbonate disappears and quenched Fe, Na-bearing dolomitic carbonatite melts were observed. For PERC3 (1.0 wt% bulk CO_2; Na_2O/CO_2 weight ratio = 0.30), the observed solidus is between 1190 and 1220 °C; for PERC (2.5 wt% bulk CO_2; Na_2O/CO_2 = 0.12), it is between 1250 and 1275 °C; and for PERC2 (5.0 wt% bulk CO_2; Na_2O/CO_2 = 0.06), it is between 1300 and 1330 °C. At 6.6 GPa, experimental solidi of natural magnesite peridotites are 100–200 °C lower than the CMAS-CO_2 solidus, chiefly owing to the fluxing effect of alkalis, and solidus temperatures increase with increasing bulk CO_2 (i.e., decreasing bulk Na_2O/CO_2), owing to dilution of Na_2O in near-solidus melt. The effects of Mg no. and Ca no. on carbonated peridotite solidi appear to be less significant than that of Na_2O/CO_2. Trends of decreasing solidus temperature with increasing Na_2O/CO_2 and with decreasing CO_2 indicate that natural mantle peridotite with ~100–1000 ppm bulk CO_2 will have solidus temperatures ~20° to ~100° lower than that determined experimentally. The solidus of peridotite drops discontinuously by ~600 °C (at 6.6 GPa) at the CO_2 bulk concentration (~5 ppm) at which carbonate is stabilized, but then varies little with increasing bulk CO_2. This result contrasts with the effect of H_2O, which lowers the solidus continuously with increasing concentration.

Keywords: Carbonated peridotite, carbonatite, mantle solidus, experimental petrology, partial melting

INTRODUCTION

High-pressure partial melting of carbonated peridotite may represent the deepest melting occurring in basalt source regions (Wyllie and Huang 1975; Galer and O'Nions 1986; Plank and Langmuir 1992). Experiments show that the solidus of carbonated peridotite intersects the oceanic geotherm at >200 km beneath ridges (Presnall et al. 2002; Dasgupta and Hirschmann 2006). However, experimental determinations may not constrain directly the partial melting behaviour of peridotite in the mantle. Studies that employ synthetic compositions (Canil and Scarfe 1990; Dalton and Presnall 1998) do not account for the influence of important oxides such as Na_2O and FeO* (= total Fe). Experiments with compositions that incorporate these components typically contain much more CO_2 than the very small concentrations (<~0.4 wt%) thought to be present in basalt source regions beneath oceanic ridges and oceanic islands, and excess CO_2 may bias experimental solidus determinations of these high variance compositions.

Estimates for the concentration of CO_2 in the mantle beneath oceanic ridges range from 50 to 2000 ppm (Saal et al. 2002). Sources beneath oceanic islands may be richer, with ~1000 to 4000 ppm CO_2 (Trull et al. 1993; Dixon et al. 1997; Pineau et al. 2004). However, owing to decarbonation of mantle xenoliths during ascent (Canil 1990) and degassing of magmas (Holloway and Blank 1994) upon eruption, significant uncertainties remain regarding average concentrations of carbon in mantle source regions (Jambon 1994). The carbon in these sources may be stored as reduced carbon (diamond or graphite), or as crystalline carbonate, depending on depth and on the oxygen fugacity (Luth 1993, 1999; Dasgupta and Hirschmann 2006), but in either case, initial melting results in stabilization of carbonatite liquid (Dasgupta and Hirschmann 2006). Therefore, determination of the onset of carbonatite stability in the presence of small amounts of carbonate is of principal importance for understanding deep melting in basalt source regions.

It is not feasible to detect experimentally the solidus of lithologies with the small amounts of carbon found in natural peridotite, so experiments are performed with much higher CO_2 concentrations (2–5 wt%) (Wendlandt and Mysen 1980; Wallace and Green 1988; Falloon and Green 1989). Because natural peridotite has high thermodynamic variance, this excess CO_2 can potentially bias experimentally determined solidi. Reaction between excess CO_2 and silicate minerals may produce more refractory crystalline carbonate compositions than those found at lower CO_2 concentration. Similarly, reaction between excess

* Present address: Lamont-Doherty Earth Observatory, Columbia University, 61 Route 9W, Palisades, New York 10964, U.S.A. E-mail: rajdeep@ldeo.columbia.edu

0003-004X/07/0203–370$05.00/DOI: 10.2138/am.2007.2201

CO_2 and silicates may consume clinopyroxene, and in extreme cases, convert lherzolitic residues to harzburgite (Wendlandt and Mysen 1980). Excess carbonate melt produced at the solidus can be diluted in incompatible solidus-lowering components such as alkalis. Experiments with natural carbonated eclogite with variable amounts and compositions of added carbonate demonstrate that initial melting temperature varies according to the composition of carbonate mineral and liquid that is stable at the solidus, (Dasgupta et al. 2005). Similar effects are expected for carbonated peridotite.

Here, we present near solidus phase equilibria experiments for three natural carbonated peridotite bulk compositions with different CO_2 contents and show that the experimental solidus depends on the quantity of CO_2 added. Using the observed trend of solidus temperatures as a function of added CO_2, we develop a conceptual model for the solidus of mantle peridotite as a function of source carbon content.

Experimental and analytical procedures

Fertile peridotite (MixKLB-1: Table 1; Dasgupta and Hirschmann 2006) rock powder was constructed from clean natural olivine, orthopyroxene, clinopyroxene, and garnet. Minerals were thoroughly mixed and ground to <5 μm in an agate mortar under ethanol. The rock powder was dried for 4 h at 1000 °C in a one-atmosphere furnace at an oxygen partial pressure approximately one order of magnitude below the buffer corresponding to quartz-magnetite-fayalite (QFM-1), fixed by a mixture of CO and CO_2 gases. The mix was then reground under ethanol, and 1.0 wt% (PERC3), 2.5 wt% (PERC), and 5.0 wt% (PERC2) CO_2 were added by mixing natural ($MgCO_3$ and $FeCO_3$) and synthetic ($CaCO_3$, Na_2CO_3, and K_2CO_3) carbonates in such a way so as to keep the Ca:Mg:Fe:Na:K of the base peridotite (MixKLB-1) unmodified (Table 1). To minimize contamination from H_2O, all the carbonate compounds were fired in a one-atmosphere furnace at 250–300 °C for 4–12 h before mixing them with silicates under ethanol. Homogeneous mixtures of carbonated peridotite were loaded in thick graphite crucibles with Pt outer capsules and kept in a drying oven at 120 °C for a couple of hours to further ensure nominally anhydrous condition before welding the outer Pt capsule. High-pressure phase-equilibria experiments were performed at 6.6 GPa in a Walker-style multi-anvil apparatus following the procedures, assemblies, and calibrations described and reported in detail by Dasgupta et al. (2004).

After the experiments, recovered capsules were mounted in epoxy, ground longitudinally, and polished on soft nylon cloth using dry polycrystalline diamond powders to achieve a 0.25 to 1 μm finish. Water and other liquid lubricants were avoided during polishing to aid preservation of carbonates. Textures of experimental charges were examined with a JEOL JXA8900R electron microprobe and a JEOL JSM-6500F FEG high-resolution SEM**.** Major-element compositions of the product phases were also obtained by WDS electron-microprobe analyses.

Table 1. Compositions (wt%) of starting materials and base peridotite

	MixKLB-1	PERC	PERC2	PERC3
SiO_2	44.54	42.29	40.05	43.63
TiO_2	0.21	0.20	0.19	0.20
Al_2O_3	3.70	3.52	3.33	3.63
Cr_2O_3	0.23	0.21	0.20	0.22
FeO*	8.08	8.07	8.07	8.08
MnO	0.14	0.13	0.13	0.14
MgO	39.30	39.26	39.22	39.27
CaO	3.52	3.52	3.51	3.52
Na_2O	0.29	0.29	0.29	0.30
K_2O	0.01	0.01	0.01	0.01
CO_2		2.51	5.01	1.02
Na_2O/CO_2		0.12	0.06	0.30
Mg no.	89.65	89.65	89.64	89.65
Ca no.	0.05	0.05	0.05	0.05

Notes: MixKLB-1 is the composition of the base peridotite. Total Fe as FeO. Mg no. = 100 × molar Mg/(Mg + Fe). Ca no. = molar Ca/(Ca + Mg + Fe).

Results

Summaries of run conditions, resulting phase assemblages, and calculated phase proportions are given in Table 2, and available compositions of quenched melt and residual minerals are detailed in Table 3. Olivine (ol), orthopyroxene (opx), and garnet (gt) appear in all the runs for all three compositions investigated. Clinopyroxene is present throughout the charge in all the runs with bulk compositions PERC3 and PERC, but for PERC2, it is absent in run M258 (6.6 GPa, 1360 °C) and it is restricted to one end of the capsule in run M242 (6.6 GPa, 1330 °C) (Table 2). Carbonate is present as magnesite solid solution (Mst_{ss}) and/or quenched carbonated melt (Fig. 1). The solidus was inferred based on textural criteria (Dasgupta and Hirschmann 2006), where discrete grains of carbonate minerals were clearly distinguished from interstitial regions of quenched carbonate-rich melts (Fig. 1). At 6.6 GPa, the solidi of PERC2, PERC, and PERC3 are located in the intervals 1300–1330, 1250–1275, and 1190–1220 °C, respectively (Fig. 2). Mst_{ss} disappears within 30–60, 25–50, and 0–25 °C of the solidus for PERC2, PERC, and PERC3, respectively (Table 2; Fig. 2). However, extended melting intervals of crystalline carbonate for runs with PERC2 and PERC are likely artifacts of the thermal gradients in the charges, as Mst_{ss} is restricted to one end of the capsule for runs M210 (PERC = 1275 °C) and M242 (PERC2 = 1330 °C). In fact, mass-balance calculations without Mst_{ss} for runs M210 (PERC = 1275 °C) and M242 (PERC2 = 1330 °C) yield quite reasonable residual sums of squares (Table 2).

Silicate mineral compositions (Table 3) change relatively little across the solidus of carbonated peridotite, except for a distinct drop in the Na_2O concentrations of cpx coinciding with textural evidence of melting (Fig. 3a). This effect diminishes with decreasing bulk carbonate concentration, corresponding to decreasing near-solidus melt fraction (Fig. 3a). These observations are consistent with preferential partitioning of Na into carbonated melt (Wallace and Green 1988; Dasgupta 2006).

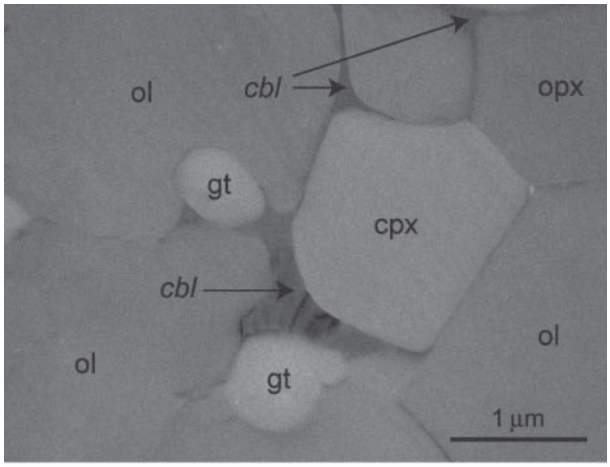

Figure 1. High-resolution secondary electron image of a representative melt-present run (M245: 6.6 GPa, 1220 °C) with bulk composition PERC3 (1 wt% CO_2). Clear evidence of quenched carbonate melt is observed in the interstices of residual olivine, opx, cpx, and garnet. Abbreviations: ol = olivine, opx = orthopyroxene, cpx = clinopyroxene, gt = garnet, and *cbl* = carbonate melt.

Changes in Mst_{ss} composition are also notable: below the solidus, it becomes progressively more calcic with increasing temperature, with Ca no. [molar Ca/(Ca + Mg + Fe)] increasing from 0.01 at 1160 °C to 0.03 at 1190 °C for experiments with PERC3 and from 0.01 at 1125 °C to 0.04 at 1250 °C for PERC (Fig. 4). For experiments with PERC2, only modest changes of Ca no. of magnesite are evident. Quenched melt pools from experiments with PERC2 have compositions similar to magnesian dolomite (Table 3; Ca no. of 0.37 to 0.41 and molar Ca/(Ca + Mg) of 0.40–0.45; Fig. 4). Reliable estimates of quenched carbonate melts from bulk compositions PERC and PERC3 could not be obtained, owing to small (<5 μm) dimensions of interstitial melt pools. However, single analyses from runs M244, M208, M245, and M243 indicate that near-solidus melts of both PERC and PERC3 are carbonatitic with ~2 wt% SiO_2, ~5 wt% FeO*, ~24 wt% MgO, and ~21 wt% CaO for PERC, and ~3.5 wt% SiO_2, ~5 wt% FeO*, ~25 wt% MgO, and ~20 wt% CaO for PERC3. Analyzed Na_2O concentrations are low (0.20–0.25 wt%; Table 3), owing to well-known difficulties in analysing alkalis from quenched carbonate melts (Yaxley and Green 1996; Dasgupta et al. 2005). However, reconstructed analyses (Table 2) based on mass balance (Yaxley and Green 1996) suggest that the carbonatite liquids are Na_2O-rich (PERC2: 1.6–1.9 wt%; PERC: 2.7–3.2 wt%; PERC3: ~4.6–5.4 wt%; Fig. 5), with Na_2O diminishing with increasing bulk CO_2.

Discussion

Melt production near the solidus of carbonated peridotite

An important consideration regarding the near-solidus melting behavior of carbonated peridotite is the proportion of melt generated near the solidus. In the experiments reported here, the phase assemblage goes from subsolidus to complete elimination of magnesite over a narrow temperature interval (25–30 °C; Fig. 2, Table 2). Consequently, the fraction of melt observed near the solidus is directly proportional to the mode of sub-solidus magnesite. Natural carbonated peridotite has high thermodynamic variance and all phases present are solutions that may vary in composition. Consequently, the actual melting relationship cannot be thermodynamically invariant, which means that experiments at smaller temperature increments or perhaps with more exacting methods of melt detection would likely reveal a finite temperature interval in which solid and liquid carbonates coexisted.

If magnesite in carbonated peridotite must melt over a finite temperature interval, a necessary corollary is that the carbonatite melt composition must evolve from the true solidus, where an infinitesimal amount of melt is present, to the exhaustion of crystalline carbonate, which occurs at ~2–12% melting in the

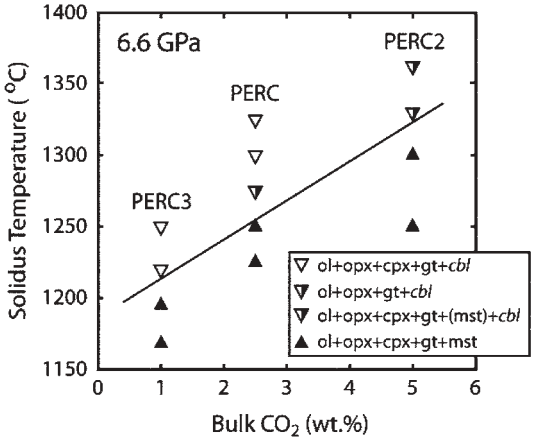

Figure 2. 6.6 GPa solidus brackets of carbonated lherzolite as a function of bulk CO_2 content. Filled, upright triangles indicate subsolidus conditions, whereas open or partially filled, inverted triangles indicate super-solidus conditions. The straight line delineates the best estimate of the solidus as a function of isochemical addition of bulk CO_2.

Table 2. Summary of run conditions, phase assemblages, and calculated phase proportions

Bulk comp.	Run no.	*T* (°C)	*t* (h)	Δlog f_{O_2}	ol	opx	cpx	gt	mst	*cbl*	sum r^2	Na_2O-melt
PERC	M205	1125	12	−1.223	57.9 (1.0)	8.0 (1.1)	14.3 (0.4)	14.8 (0.6)	5.0 (0.1)	–	0.03	
	M207	1225	12	−1.148	59.4 (0.6)	7.9 (1.0)	14.3 (0.5)	13.6 (0.4)	4.7 (0.1)	–	0.15	
	M213	1250	12	−1.135	60.1 (0.8)	8.1 (0.5)	13.6 (0.2)	13.3 (0.4)	4.9 (0.1)	–	0.18	
	M210*	1275	12	−1.119	58.7 (0.6)	15.4 (0.5)	7.5 (0.3)	12.1 (0.6)	+	6.2 (0.1)	0.05	3.2 (0.1)
	M244	1300	12		57.3 (0.4)	16.3 (0.5)	7.8 (0.3)	12.4 (0.4)	–	6.2 (0.1)	0.02	2.8 (0.1)
	M208	1325	12		56.9 (0.6)	15.7 (0.7)	7.5 (0.3)	13.6 (0.3)	–	6.2 (0.1)	0.03	2.7 (0.1)
PERC2	M259	1250	24	−1.125	55.1 (0.8)	6.0 (1.0)	14.5 (0.4)	14.4 (0.4)	9.9 (0.1)	–	0.09	
	M241	1300	12	−1.104	55.1 (0.8)	6.3 (0.8)	14.6 (0.4)	13.9 (0.2)	10.1 (0.1)	–	0.10	
	M242*	1330	12	−1.080	55.2 (1.5)	20.1 (1.7)	0.2 (0.7)	13.0 (0.5)	+	11.6 (0.6)	0.01	1.9 (0.1)
	M258	1360	12		54.0 (0.8)	19.6 (0.7)	-	15.3 (0.4)	–	11.1 (0.2)	0.07	1.6 (0.1)
PERC3	M247	1160	24	−1.195	60.8 (0.6)	7.9 (0.6)	15.5 (0.6)	13.7 (0.3)	2.1 (0.1)	–	0.54	
	M246	1190	24	−1.191	60.8 (0.5)	7.8 (0.6)	15.3 (0.3)	13.9 (0.2)	2.1 (0.0)	–	0.35	
	M245	1220	16		61.0 (1.1)	12.0 (1.4)	12.8 (0.4)	11.7 (0.6)	–	2.6 (0.2)	0.17	5.4 (0.5)
	M243	1250	12		62.3 (1.2)	10.7 (0.9)	12.8 (0.4)	11.3 (0.6)	–	2.9 (0.2)	0.43	4.6 (0.5)

Notes: ol = olivine, opx = orthopyroxene, cpx = clinopyroxene, gt = garnet, mst = magnesite solid solution, *cbl* = carbonate-rich melt; weight fractions are by mass balance calculation using all the oxide concentrations of constituent phases except for melt present runs where only CaO, MgO, FeO, SiO_2, and CO_2 were used of the phases for the calculation; values within parentheses are 1σ standard deviation with respect to mean for the calculated phase proportions, using uncertainties in analyzed phase compositions (Table 3); "sum r^2" is the summation of squares of residuals obtained by using mineral modes, phase compositions, and composition of the starting materials. Concentration of Na_2O in the melt is estimated based on mass balance approach of Yaxley and Green (1996) using concentration of other oxides in the constituent phases, estimated phase proportions, and the composition of the starting materials. *Presence of magnesite in these experiments is noted in trace amount only on one end of the capsule and is believed to be stable due to slightly lower temperature than the nominal temperature of the experiment at this portion of the capsule; low sum of squared residuals in mass balance calculation without involving magnesite, confirms that magnesite is not likely to be an equilibrium phase at these run conditions. Oxygen fugacity calculation is done using the EMOD buffer (Olafsson and Eggler 1983; Luth 1993) using the measured phase compositions from the experiments. Activities for mineral end-members have been calculated with the program AX. Values are reported as Δlog f_{O_2}, defined as logf_{O_2} (sample) – logf_{O_2} (FsMC) (Luth 1993).

TABLE 3. Equilibrium phase compositions from 6.6 GPa experiments with differenet CO_2 bearing peridotite bulk compositions

Run no.	Phase	n†	SiO_2	TiO_2	Al_2O_3	Cr_2O_3	FeO*	MnO	MgO	CaO	Na_2O	K_2O	CO_2‡	Total	Mg no.
PERC															
M205	Ol	11	40.75(58)	0.06(3)	0.20(13)	0.01(3)	9.79(17)	0.10(5)	48.92(56)	0.19(17)	0.04(2)	0.02(1)		100.08	89.90
	Opx	8	57.71(88)	0.10(3)	0.83(34)	0.07(6)	6.05(21)	0.11(5)	34.49(30)	0.74(2)	0.14(3)	0.02(1)		100.25	91.04
	Cpx	10	55.09(69)	0.19(3)	1.86(19)	0.26(3)	3.70(13)	0.10(5)	19.02(38)	18.35(27)	1.14(8)	0.02(1)		99.73	90.15
	Gt	7	41.79(89)	0.91(9)	20.55(98)	0.80(8)	9.06(40)	0.33(7)	21.83(85)	4.59(23)	0.09(2)	0.03(2)		99.98	81.10
	Mst_{ss}	3	0.17(7)	0.01(2)	0.02(3)	0.09(2)	3.52(1)	0.08(7)	44.34(63)	0.86(10)	0.02(3)	0.03(2)	51.21	100.34	95.74
M207	Ol	11	40.43(48)	0.05(2)	0.08(8)	0.03(3)	9.86(12)	0.12(5)	48.76(37)	0.09(3)	0.02(2)	0.02(2)		99.44	89.82
	Opx	10	57.38(65)	0.10(3)	1.08(24)	0.06(3)	6.10(14)	0.10(6)	34.60(73)	0.88(13)	0.12(2)	0.02(2)		100.05	91.00
	Cpx	12	55.20(39)	0.19(4)	1.91(34)	0.24(5)	3.86(19)	0.14(6)	18.99(61)	18.16(69)	1.11(7)	0.02(2)		99.83	89.77
	Gt	5	41.78(12)	0.91(9)	21.61(44)	0.94(4)	8.94(36)	0.34(5)	20.15(53)	4.95(28)	0.05(2)	0.02(2)		99.70	80.06
	Mst_{ss}	6	0.04(2)	0.02(2)	0.01(2)	0.02(3)	5.01(44)	0.13(4)	42.12(62)	2.02(27)	0.01(1)	0.02(1)	50.72	50.72	93.75
M213	Ol	11	40.95(25)	0.06(4)	0.26(20)	0.04(3)	9.81(15)	0.11(4)	48.30(50)	0.23(15)	0.02(2)	0.02(1)		99.79	89.77
	Opx	11	56.91(67)	0.15(3)	1.40(99)	0.09(6)	6.11(19)	0.14(3)	34.03(95)	0.95(10)	0.13(3)	0.01(2)		100.11	90.85
	Cpx	17	54.95(30)	0.20(5)	2.05(17)	0.23(4)	3.84(11)	0.13(4)	19.31(53)	17.81(44)	1.09(4)	0.02(2)		99.64	89.96
	Gt	8	41.64(40)	0.86(11)	21.13(28)	0.96(10)	8.72(46)	0.28(5)	20.01(35)	5.15(24)	0.08(3)	0.01(1)		98.84	80.35
	Mst_{ss}	6	0.29(18)	0.02(3)	0.03(5)	0.04(5)	5.51(14)	0.16(5)	41.43(39)	2.36(10)	0.03(3)	0.01(1)	50.54	100.44	93.06
M210	Ol	21	41.15(22)	0.04(4)	0.09(7)	0.03(2)	9.78(21)	0.11(5)	48.60(47)	0.15(9)	0.02(2)	0.02(2)		99.97	89.86
	Opx	10	57.34(35)	0.15(5)	0.86(9)	0.08(4)	5.93(14)	0.10(4)	34.14(27)	1.17(9)	0.12(4)	0.02(1)		99.91	91.12
	Cpx	19	55.42(31)	0.22(6)	2.06(28)	0.22(6)	3.80(11)	0.12(3)	19.81(74)	17.84(32)	0.94(6)	0.02(1)		100.44	90.30
	Gt	9	41.67(52)	0.86(9)	21.46(47)	0.95(5)	8.51(23)	0.30(4)	20.37(45)	5.20(12)	0.04(2)	0.02(2)		99.38	81.00
	Mst_{ss}	4	0.34(13)	0.02(2)	0.03(3)	0.01(1)	5.37(20)	0.19(6)	41.18(65)	2.75(11)	0.04(2)	0.01(1)	50.52	100.44	93.19
M244	Ol	11	40.81(21)	0.02(1)	0.02(1)	0.01(1)	9.72(21)	0.12(2)	49.12(23)	0.10(3)	0.05(2)	0.02(1)		99.99	90.01
	Opx	10	57.19(12)	0.10(3)	0.83(14)	0.07(3)	5.92(19)	0.13(3)	34.19(22)	1.20(11)	0.12(3)	0.03(1)		99.78	91.15
	Cpx	14	55.08(51)	0.21(7)	2.00(43)	0.20(5)	3.89(17)	0.11(3)	20.04(66)	17.30(79)	0.92(10)	0.02(1)		99.77	90.19
	Gt	9	41.93(39)	0.70(19)	22.12(36)	1.05(11)	8.63(21)	0.27(4)	20.16(14)	5.21(31)	0.06(3)	0.03(1)		100.01	80.59
M208	Ol	12	40.98(24)	0.03(3)	0.04(3)	0.02(2)	9.68(13)	0.13(4)	49.42(29)	0.10(2)	0.05(1)	0.02(2)		100.46	90.10
	Opx	13	57.37(32)	0.10(5)	0.87(7)	0.07(4)	5.88(13)	0.13(2)	34.16(23)	1.30(13)	0.14(4)	0.03(1)		100.04	91.20
	Cpx	19	55.21(43)	0.21(7)	2.09(50)	0.20(6)	3.97(18)	0.11(3)	20.34(69)	17.02(87)	0.91(9)	0.02(1)		100.06	90.14
	Gt	10	41.93(20)	0.60(21)	22.32(64)	1.05(17)	8.83(60)	0.27(6)	20.10(72)	5.11(33)	0.06(2)	0.03(2)		100.31	80.23
PERC2															
M259	Ol	11	40.91(54)	0.02(1)	0.11(6)	0.03(1)	9.50(24)	0.14(3)	49.16(42)	0.16(5)	0.06(4)	0.04(2)		100.10	90.22
	Opx	7	56.09(82)	0.08(5)	1.19(83)	0.08(1)	6.05(16)	0.11(5)	35.83(82)	1.15(28)	0.15(7)	0.05(4)		100.77	91.35
	Cpx	13	55.05(73)	0.19(15)	2.24(29)	0.21(7)	3.82(32)	0.10(4)	19.55(54)	17.68(74)	1.01(11)	0.02(2)		99.87	90.12
	Gt	9	42.81(20)	0.62(20)	20.78(58)	0.90(12)	8.65(52)	0.31(8)	21.03(56)	4.79(24)	0.08(5)	0.02(2)		99.98	81.25
	Mst_{ss}	8	0.09(6)	0.02(2)	0.01(1)	0.04(2)	4.80(91)	0.13(8)	42.37(54)	1.92(58)	0.12(8)	0.01(2)	50.78	100.29	94.03
M241	Ol	15	40.95(21)	0.02(2)	0.07(6)	0.03(3)	10.14(16)	0.12(4)	49.25(34)	0.11(3)	0.03(2)	0.02(1)		100.74	89.64
	Opx	10	57.47(29)	0.11(3)	0.77(9)	0.08(3)	6.09(9)	0.11(5)	34.09(57)	1.16(8)	0.15(3)	0.03(1)		100.05	90.90
	Cpx	10	55.41(46)	0.14(4)	2.19(34)	0.15(5)	3.93(21)	0.10(2)	19.45(37)	17.65(50)	1.13(8)	0.03(1)		100.18	89.82
	Gt	7	42.16(31)	0.81(19)	21.25(75)	1.00(5)	8.84(46)	0.29(6)	20.90(87)	4.84(21)	0.08(2)	0.02(2)		100.20	80.83
	Mst_{ss}	6	0.05(3)	0.02(2)	0.02(3)	0.06(7)	5.52(83)	0.13(4)	41.65(82)	2.09(47)	0.05(5)	0.02(2)	50.61	100.23	93.08
M242	Ol	11	40.57(40)	0.03(1)	0.13(6)	0.00(1)	9.83(11)	0.14(2)	48.54(31)	0.17(3)	0.03(1)	0.02(1)		99.45	89.80
	Opx	13	57.63(40)	0.11(3)	0.76(8)	0.08(4)	5.89(15)	0.10(4)	34.04(63)	1.21(20)	0.15(2)	0.02(2)		99.97	91.15
	Cpx	13	55.49(71)	0.13(9)	1.45(19)	0.21(3)	3.11(19)	0.13(4)	22.09(37)	16.55(39)	0.80(6)	0.02(2)		100.08	92.69
	Gt	9	42.10(16)	0.64(13)	21.65(41)	1.13(12)	8.99(19)	0.31(21)	20.30(34)	4.50(13)	0.10(5)	0.03(3)		99.75	80.10
	Mst_{ss}	8	0.02(2)	0.01(3)	0.01(2)	0.03(3)	4.89(12)	0.09(5)	42.01(91)	2.52(28)	0.03(3)	0.01(1)	50.49	100.11	93.87
	Cbl	7	4.4(29)	0.24(28)	1.0(11)	0.04(4)	5.29(93)	0.19(6)	23.8(30)	22.1(40)	0.25(16)	0.02(2)	42.7(27)	100.00	88.93
M258	Ol	15	40.64(31)	0.01(1)	0.03(3)	0.02(1)	9.33(16)	0.10(6)	49.77(33)	0.12(3)	0.11(4)	0.03(3)		100.16	90.49
	Opx	14	57.21(27)	0.04(2)	0.79(3)	0.07(2)	5.87(16)	0.09(5)	34.68(70)	1.30(19)	0.17(5)	0.02(3)		100.24	91.33
	Gt	10	43.57(65)	0.49(20)	20.52(61)	1.12(12)	8.14(53)	0.26(8)	21.21(58)	4.91(25)	0.14(3)	0.01(1)		100.39	82.28
	Cbl	5	2.58(29)	0.05(5)	0.57(9)	n.d.	5.91(63)	0.20(1)	21.4(20)	24.0(19)	0.20(1)	0.01(1)	45.0(20)	100.00	86.60
PERC3															
M247	Ol	6	40.60(21)	0.03(3)	0.15(08)	0.02(5)	10.15(13)	0.10(5)	48.67(52)	0.28(29)	0.02(1)	0.03(2)		100.05	89.41
	Opx	7	57.59(20)	0.11(3)	0.59(12)	0.12(6)	6.11(13)	0.12(3)	34.75(25)	0.71(8)	0.11(4)	0.02(1)		100.23	91.02
	Cpx	13	55.33(57)	0.23(3)	1.83(14)	0.25(4)	3.72(27)	0.11(5)	19.52(79)	17.89(85)	1.19(6)	0.02(1)		100.08	90.35
	Gt	4	41.39(3)	0.71(17)	22.64(3)	0.91(3)	9.88(23)	0.32(1)	19.56(25)	4.71(11)	0.06(2)	0.02(1)		100.20	77.92
	Mst_{ss}	4	0.09(8)	0.03(4)	0.00	0.02(2)	4.98(2)	0.14(4)	42.74(62)	1.30(7)	0.03(3)	0.02(2)	50.84	100.18	93.86
M246	Ol	6	40.91(12)	0.06(4)	0.10(12)	0.04(4)	10.11(9)	0.12(3)	49.01(21)	0.09(3)	0.03(2)	0.03		100.50	89.63
	Opx	8	57.71(51)	0.11(6)	0.64(19)	0.08(4)	6.25(8)	0.10(3)	34.87(33)	0.72(8)	0.13(2)	0.03(2)		100.62	90.87
	Cpx	11	55.30(78)	0.19(4)	1.69(17)	0.25(5)	3.78(10)	0.14(7)	19.55(54)	17.69(55)	1.17(6)	0.02(1)		99.78	90.22
	Gt	3	41.67(30)	0.89(9)	22.51(24)	0.98(1)	9.39(39)	0.33(2)	19.59(36)	4.76(16)	0.11(3)	0.02(2)		100.25	78.80
	Mst_{ss}	4	0.12(3)	0.01(2)	0.02(3)	0.01(1)	5.26(38)	0.15(6)	41.99(29)	1.89(15)	0.05(3)	0.02(1)	50.70	100.23	93.43
M245	Ol	10	40.57(90)	0.04(4)	0.10(12)	0.03(4)	10.07(24)	0.10(3)	48.71(64)	0.08(3)	0.04(2)	0.02(2)		99.78	89.61
	Opx	6	57.36(50)	0.11(4)	0.95(60)	0.09(6)	6.08(14)	0.12(5)	33.93(58)	1.06(10)	0.14(6)	0.03(2)		99.90	90.86
	Cpx	10	55.50(39)	0.19(7)	1.65(48)	0.24(7)	3.84(15)	0.10(4)	19.61(53)	17.87(38)	1.04(5)	0.02(2)		100.07	90.11
	Gt	5	42.11(42)	0.93(7)	22.33(13)	0.99(6)	8.80(17)	0.35(8)	20.59(40)	4.73(20)	0.06(4)	0.03		100.90	80.66
M243	Ol	7	41.21(44)	0.07(2)	0.11(9)	0.05(4)	10.43(12)	0.11(5)	48.27(85)	0.27(11)	0.06(5)	0.01(2)		100.60	89.19
	Opx	6	57.19(76)	0.12(2)	1.00(45)	0.13(6)	6.23(26)	0.15(4)	33.87(85)	1.09(11)	0.13(1)	0.02(2)		99.93	90.65
	Cpx	10	55.36(51)	0.20(4)	1.77(30)	0.25(4)	3.91(6)	0.10(3)	19.52(72)	17.78(70)	1.01(7)	0.04(2)		99.94	89.89
	Gt	3	42.15(33)	0.73(11)	22.63(31)	1.02(8)	8.13(25)	0.27(4)	20.46(31)	4.52(19)	0.10(3)	0.03(2)		100.05	81.76

Notes: Because of very small dimensions (<5 μm) of the interstitial melt pools for runs with bulk compositions PERC3 and PERC, melt compositions for these are not reported in here; estimates based on single analysis from each are given in the text. Units in parentheses represent 1σ standard deviations in terms of least units cited on the basis of replicate analyses. 40.75(58) should be read as 40.75 ± 0.58. Concentrations of Na_2O in *Cbl* are as measured and believed to be underestimates due to well-known problems of alkali loss during sample preparations of quenched carbonate melts bearing runs (e.g., Yaxley and Green 1996; Dasgupta et al. 2005); the corrected values of Na_2O in carbonate melts are given in Table 2. † Number of analyses averaged. ‡ CO_2 is calculated by difference of 100 and the measured analytical total for carbonate melt and by stoichiometry for magnesite.

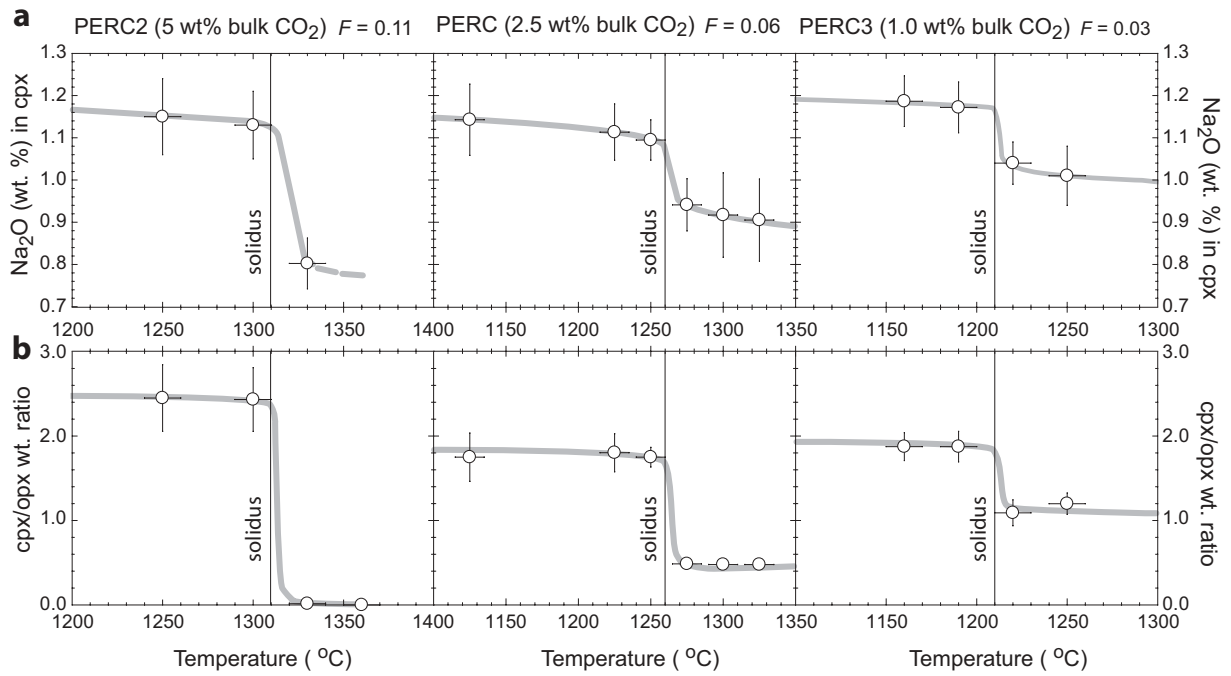

FIGURE 3. Variations of Na_2O concentrations in cpx (**a**) and cpx/opx weight ratio (**b**) as a function of temperature across the solidi of three different carbonated lherzolite bulk compositions, PERC2 (5.0 wt% bulk CO_2), PERC (2.5 wt% bulk CO_2), and PERC3 (1.0 wt% bulk CO_2). Error bars of Na_2O concentrations in **a** are 1σ of multiple analyses from each experiment (Table 3) and error bars of cpx/opx ratios in **b** are based on uncertainties in phase proportions from mass-balance calculations (Table 2). The decrease in Na_2O in cpx across the solidus relates to formation of Na_2O-rich carbonatite melts. The sharp decreases in Na concentration in cpx and in cpx/opx ratio coincide with textural evidence of melting, and the magnitude of the changes diminishes systematically with decreasing bulk CO_2 composition, consistent with decreasing carbonatitic melt fraction (F) produced near the solidus, 11% for PERC2, 6% for PERC, and 3% for PERC3 (Table 2). The decreased cpx/opx ratio across the solidus is indicative of the peritectic melting reaction (see text, Eq. 5).

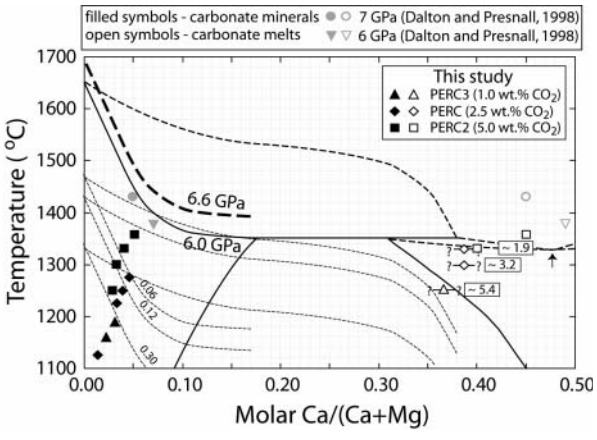

FIGURE 4. Comparison of phase relations for the Ca-poor part of the system $CaCO_3$–$MgCO_3$ at 6 GPa (Buob et al. 2006) to the projected composition of carbonate minerals (solid symbols) and melts (open symbols) along the $CaCO_3$-$MgCO_3$ pseudobinary from the different natural carbonated peridotite compositions used in this study (at 6.6 GPa) and from the study of Dalton and Presnall (1998) in model CMAS-CO_2 peridotite system (at 6 and 7 GPa). The arrow points to the location of the CM-CO_2 minimum from the study of Buob et al. (2006). The solidus temperature of CMAS-CO_2 peridotite (Dalton and Presnall 1998) is similar to the minimum in CM-CO_2 (Buob et al. 2006), because the temperature of the solidus for pure Ca-Mg carbonate varies by less than 50 °C for compositions with Ca no. between 0.10 and 0.50 (Buob et al. 2006). The compositions of carbonate crystals and melts from this study and that in the CMAS-CO_2 system (Dalton and Presnall 1998) are broadly consistent with the topology of the melting loop in the CM-CO_2 binary at similar pressure i.e., melts of higher Ca/Mg coexist with crystalline carbonate of lower Ca/Mg; however, in detail, the melt compositions from CMAS-CO_2 are more calcic than predicted from the CM-CO_2 phase relations. Compositions of carbonate crystals and melts from natural carbonated peridotite at 6.6 GPa are also similar in terms of Ca/Mg systematics, but the solidi for respective bulk compositions are shifted to lower temperatures with respect to CMAS-CO_2 and CM-CO_2 solidi; bold dashed curve represents the 6.6 GPa solidus of CM-CO_2, adjusted from the 6 GPa data of Buob et al. (2006) by extrapolation and using the lower pressure data from Byrnes and Wyllie (1981) and Irving and Wyllie (1975). The thin dashed lines are inferred projected locations of carbonated peridotite solidi for different Na_2O/CO_2 ratios (marked against the lines) assuming that the topology of the solidi as a function of variable Ca/Mg for natural peridotite + CO_2 are similar to that of CM-CO_2 solidus (Buob et al. 2006) at similar pressure. The numbers against the projected melt compositions from this study are estimated concentrations of Na_2O in the melt; increased Na concentration in near-solidus melts from PERC2 to PERC3 is consistent with the decreased solidi temperature.

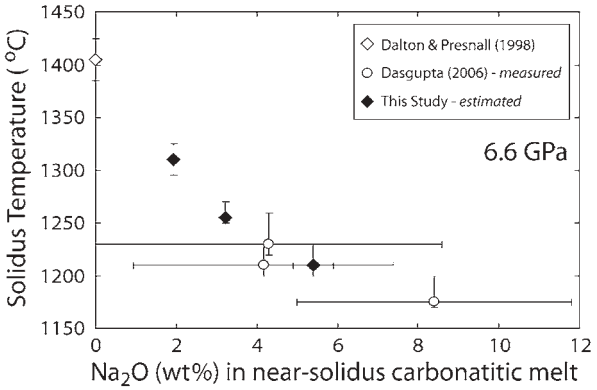

FIGURE 5. 6.6 GPa solidus brackets of carbonated peridotite vs. Na_2O concentrations (wt%) in near-solidus carbonate melts. Data are from this study, from peridotite-carbonate melt sandwich experiments (Dasgupta 2006), and from Dalton and Presnall (1998). The near-solidus melt Na_2O concentrations in this study are estimates, based on the mass-balance approach of Yaxley and Green (1996). The errors in estimated Na_2O concentrations from this study are derived from propagating the errors in estimated phase proportions. The data from sandwich experiments were determined by electron-microprobe analysis using a broad-beam technique. Combining all data, a trend of decreasing isobaric solidus temperatures with increasing Na concentrations of near-solidus melts is evident.

experiments reported here. Possible compositional variations include shifts in the chief oxides in carbonatite liquids (CaO, MgO, and FeO), changes in concentrations of oxides that reside mainly in the silicate minerals of peridotite (SiO_2, TiO_2, and Al_2O_3), or in minor components that are incompatible in the silicate minerals and therefore concentrate in small degree liquids (Na_2O, K_2O, and H_2O). If variations in the extent of melting and temperature are small, major oxide (CaO, MgO, and FeO) concentrations will not change significantly because they are buffered by Ca-Mg and Mg-Fe exchange reactions between carbonatite liquid and residual olivine, pyroxenes, and garnet. Similarly, SiO_2 and Al_2O_3 concentrations in the liquid are unlikely to change appreciably, as their activities are buffered by reactions between those silicate minerals. On the other hand, concentrations of components incompatible in the minerals (Na_2O, K_2O, and H_2O) can change dramatically with melt fraction, as they are enriched at the solidus and become diluted with increasing melt fraction. A key point is that such variations in liquid composition are likely to be minimized when the total carbonate present is small. Thus, we expect that the finite carbonate melting interval will be greatest for experimental bulk compositions with relatively large amounts of carbonate.

Because we do not have definite evidence of coexisting stable carbonatite liquid and crystalline carbonate, our experiments do not capture the possible subtle changes in melt composition or phase proportions near the solidus of carbonated peridotite. Either those changes occur between our observed sub-solidus and magnesite-out brackets (Fig. 2) or there are small amounts of undetected alkali-rich liquid present in experiments that we record as sub-solidus. If the latter is true, then the sharp decrease in Na concentration of residual clinopyroxene indicates the apparent solidus, which coincides with the major melting interval of magnesite, instead of the true solidus. However, the experiments still place strong constraints on the melting behavior of natural carbonated peridotite with natural concentrations of CO_2 if we recognize that this carbonate-melting interval diminishes with decreasing CO_2. In other words, the trend depicted in Figure 2 defines unambiguously the relation between bulk CO_2 and the temperature of magnesite exhaustion that, extrapolated to the low CO_2 concentrations expected in nature (100–4000 ppm), must converge with the true carbonated peridotite solidus.

Effect of CO_2 concentration on the carbonated peridotite solidus

Perhaps the most surprising result of these experiments is that apparent solidus temperatures of carbonated peridotite increase with increasing bulk CO_2. Generally volatile elements diminish rock solidi, and so one might expect that larger amounts should have progressively greater effect on the solidus. This is not the case for two reasons: First, except at very low concentrations (Keppler et al. 2003), CO_2 is stored in a carbonate mineral. Thus, changes in bulk CO_2 do not increase the CO_2 fugacity, because the latter is fixed by reactions similar to

$$\underset{\text{ol}}{Mg_2SiO_4} + CO_2 \leftrightarrow \underset{\text{opx}}{MgSiO_3} + \underset{\text{mst}}{MgCO_3} \quad (1)$$

Second, the initial melt formed from carbonated peridotite is carbonatitic, meaning that the composition of the near-solidus liquid is not a strong function of the amount of carbonate mineral present.

The observed increase in solidus temperature with increasing total CO_2 is related to the detailed changes in near-solidus liquid composition, as has also been found for partial melting of carbonated eclogite (Dasgupta et al. 2005). The solidus temperature of carbonated peridotite is influenced chiefly by two compositional effects. The first pertains to Ca no. of coexisting melts and near-solidus Mst_{ss}, and the second relates to the concentration of Na_2O in the near-solidus carbonatitic melt. As in the case of carbonated eclogite, the detailed effects of added CO_2 on the peridotite solidus depend on the compositional changes associated with CO_2 addition. For the experiments in this study, CO_2 was added as carbonate such that the relative proportions of major-element cations (Ca, Mg, Fe, Na, K) were held constant, but, with increasing bulk CO_2, the ratio of Na_2O to CO_2 diminishes. In nature, variations in CO_2 relative to major cations may not be similarly isochemical.

The solidi detected for carbonated lherzolites in this study are cooler than those found from simple analogue (CMAS) compositions (Fig. 6). This difference must reflect the influence of additional components such as Na_2O and FeO*, as these have the largest concentrations in near-solidus carbonatitic liquids (Table 3). The influence of FeO* is difficult to gauge independently, as there are few data that allow one to infer the relationship between solidus temperature and liquid or bulk FeO* concentration. On the other hand, observed solidus temperatures for PERC2, PERC, and PERC3 diminish with increasing Na_2O in the liquid (Table 2; Fig. 5) suggesting a key role for Na, as was also found for partial melting of carbonated eclogite (Dasgupta et al. 2005). The Na_2O concentration of near-solidus

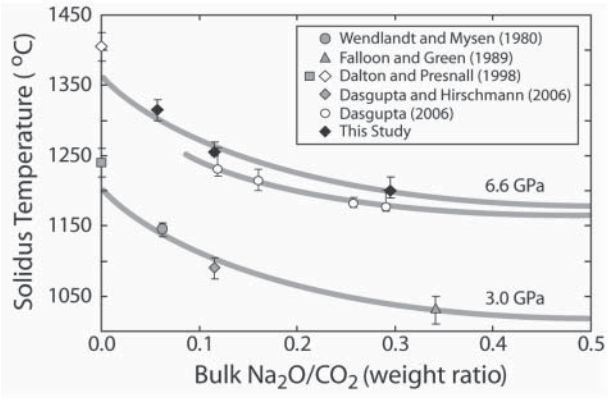

FIGURE 6. Solidus temperatures vs. Na_2O/CO_2 weight ratio of bulk starting materials for both natural and simple peridotite+CO_2 systems at 6.6 (black and white symbols). Data at 6.6 GPa include constraints from PERC peridotites (black symbols, this study), solidus brackets from peridotite-carbonate melt sandwich experiments (Dasgupta 2006), and an estimated solidus bracket for CMAS-CO_2 peridotite interpolated from the 6 and 7 GPa data of Dalton and Presnall (1998). Also shown are solidus brackets at 3.0 GPa (gray symbols) using data from previous experimental studies (Wendlandt and Mysen 1980; Falloon and Green 1989; Dalton and Presnall 1998; Dasgupta and Hirschmann 2006). The bulk compositions of the carbonate-melt-peridotite sandwich experiments have Ca/(Ca + Mg + Fe*) = 0.08–0.10 (Dasgupta 2006), in contrast to the PERC experiments, which have Ca/(Ca + Mg + Fe*) = 0.05. The drawn curves of solidus vs. Na_2O/CO_2 do not pass through the Fe-free solidus estimate of Dalton and Presnall (1998), which probably has a slightly higher solidus than expected in more complex Fe-bearing compositions.

partial melts increases with increased availability of Na_2O in the bulk rock and diminishes with increasing proportion of carbonatite melt produced near the solidus. The latter is proportional to the amount of available carbonate, and therefore, assuming that carbonate minerals are eliminated from the residue near the solidus, the apparent solidus temperature should diminish with increasing bulk Na_2O/CO_2 ratio.

The effect of bulk Na_2O/CO_2 ratio on solidi of carbonated peridotite and its role relative to other compositional variables is evident in Figure 6, which depicts solidi as a function of bulk Na_2O/CO_2 for three sets of experiments. These experiments include those determined in this study at 6.6 GPa, experiments on carbonated peridotite at 3 GPa (Wendlandt and Mysen 1980; Falloon and Green 1989; Dalton and Presnall 1998; Dasgupta and Hirschmann 2006), and a separate series of determinations at 6.6 GPa from peridotite-carbonatite sandwich experiments (Dasgupta 2006) that employed bulk compositions more calcic than the PERC series. The PERC bulk compositions have Ca no. = 0.05, similar to typical fertile peridotite, which normally has Ca no. = 0.05 ± 0.01 (Herzberg et al. 1988). The compositions from Dasgupta (2006) have Ca no. = 0.08–0.10. Each series shows decreasing solidus temperatures with increasing Na_2O/CO_2, reflecting enhanced Na_2Oin near-solidus liquids (Fig. 5). The small difference in trends at 6.6 GPa between the bulk compositions with differing Ca no. suggests that Na_2O/CO_2 has greater influence on the carbonated peridotite solidus than Ca no. The larger influence of Ca no. on carbonated eclogite solidi (Dasgupta et al. 2005) likely reflects much greater variability of Ca no. in eclogites relative to peridotites. Note also that the trends at each pressure are displaced to lower temperature by a small amount relative to relevant solidi for CMAS-CO_2 peridotite (Dalton and Presnall 1998). The offset may reflect a small solidus depression in the natural-composition experiments caused by FeO*.

An important feature of the trends in the solidus with increasing Na_2O/CO_2, depicted in Figure 7, is that their slopes diminish at higher values of Na_2O/CO_2. Because natural fertile lherzolite with ~0.3 wt% Na_2O likely has very high values of Na_2O/CO_2 (between 0.75 and 30 for 100–4000 ppm CO_2) compared to those explored experimentally (<0.35; Fig. 6), variations in CO_2 among natural peridotites with similar bulk Na_2O contents may have little influence on solidus temperatures. This would not be unexpected because the concentration of Na_2O in near-solidus partial melts (Fig. 5) must reach a limit given by $C_0/D^{perid/cbl}$, where C_0 is the concentration of Na_2O in the bulk peridotite and $D^{perid/cbl}$ is the bulk partition coefficient of Na_2O between peridotite residual minerals and carbonatite liquid. Thus, whereas the Na_2O contents of near-solidus carbonatitic partial melts can be quite variable in experiments (Fig. 5), owing in small part to variations in bulk Na_2O and in large part to differences bulk CO_2 leading to variations in near-solidus melt fractions, it may vary much less in natural carbonated peridotites.

The chief reservoir of Na_2O in carbonated peridotite is clinopyroxene. As illustrated in Figure 3, at 6.6 GPa, Na_2O in clinopyroxene diminishes when carbonate melt is stable, meaning that Na_2O is incompatible in clinopyroxene under these conditions. Comparison of Na_2O concentrations in clinopyroxene (Table 3) with Na_2O concentrations estimated in coexisting near-solidus liquids by calculated mass balance (Table 2) suggest values of $D_{Na}^{cpx/cbl} = 0.23–0.42$, in good agreement with partition coefficients of 0.15–0.39 and 0.15 measured, respectively, from carbonated peridotite sandwich experiments at 6.6 GPa (Dasgupta 2006) and 3 GPa (Wallace and Green 1988). Na_2O is less compatible in other residual minerals, which have mineral/liquid partition coefficients ranging from ~0.004 (for olivine) to ~0.04 (for orthopyroxene) (calculated from mineral and liquid Na_2O concentrations in Tables 2 and 3), but have a modest effect on the bulk partition coefficient owing to their large total modes. For a natural carbonated peridotite with 0.3 wt% Na_2O, 60% olivine, 10% opx, 15% gt, and 15% cpx (Table 2), an appropriate bulk $D^{perid/cbl}$ for Na is ~0.06 and the near-solidus liquid has ~5 wt% Na_2O. Larger enrichments in near-solidus Na_2O are possible for bulk compositions with unusually high Na_2O (Dasgupta 2006) (Fig. 5).

As noted above, melting of residual crystalline carbonate from carbonated peridotite likely occurs over a finite melting interval, and our experiments do not capture the melt compositions at true near-solidus ($F = 0$) conditions. Thus, the influence of variations in bulk CO_2 on melt composition and solidus temperature for true near-solidus liquids requires further consideration. For magnesite peridotite with otherwise identical composition (i.e., the same bulk oxide compositions), differences in bulk CO_2 should produce residues with variations in silicate mineral modes (i.e., reaction 1), but for small amounts of added CO_2, this should not

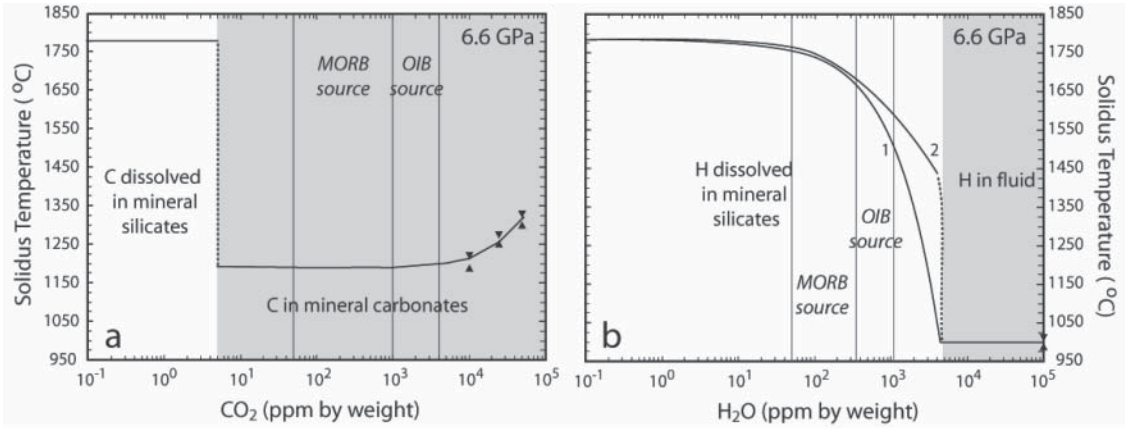

FIGURE 7. Illustration of the solidus of natural peridotite as a function of increasing bulk CO_2 (**a**) and H_2O (**b**) content at a pressure similar to 6.6 GPa. (**a**) The solidus of peridotite with up to ~5 ppm CO_2 remains almost identical to that of C-free peridotite (Hirschmann 2000), as C remains soluble in nominally C-free peridotitic mineral assemblages up to this concentration (Keppler et al. 2003) and has negligible effect on freezing point depression (<5 °C) of the peridotite solidus. When the storage capacity of carbon in peridotitic minerals is exceeded, magnesite is stabilized (provided conditions are sufficiently oxidizing) and the solidus of carbonated lherzolite drops by ~600 °C. The solidus changes little with further increases in bulk CO_2 until concentrations similar to those employed in the present experiments are reached, at which point it apparently increases, assuming that the increased CO_2 concentration is not accompanied by large increases in alkalis. The solidus of carbonated peridotite as a function of variable CO_2 concentration is a linear fit through 6.6 GPa solidus brackets (inverted and upright triangles). (**b**) The solidus of peridotite with increasing bulk water content has been parameterized from Katz et al. (2003) (curve 1) and from Aubaud et al. (2004), following the cryoscopic approximation described in Hirschmann et al. (1999) (curve 2). Curve 1 is calculated from Equation 16 of Katz et al. (2003), $\Delta T\,(X_{H_2O}) = KX^{\gamma}_{H_2O}$, where ΔT is the difference between the solidus with H_2O added and that of dry peridotite (taken from Hirschmann 2000), X_{H_2O} was the concentration of water in the liquid present at the solidus, and K and γ are empirical parameters from Katz et al. (2003). Values of X_{H_2O} were calculated for a range of bulk water contents using the batch melting equation for $F = 0$ and value of 0.009 for the bulk partition coefficient for water (Aubaud et al. 2004). Hydrous solidi diminish until the H_2O storage capacity of solid peridotite is reached at ~4000 ppm H_2O (Hirschmann et al. 2005) and ~1000 °C (Kawamoto and Holloway 1997; indicated by brackets along the right-hand axis of the diagram). The key distinction between the effects of CO_2 and H_2O is that there is a sharp discontinuity in the solidus when CO_2 is added whereas H_2O addition causes the solidus to diminish continuously.

have large effects on bulk partition coefficients. Consequently, true near-solidus melts of such peridotites should have similar Na_2O contents, irrespective of total CO_2 concentrations and therefore may have similar true solidi. However, with increasing bulk CO_2, the melt fraction present at the point of exhaustion of magnesite increases, and consequently, liquids become depleted in Na_2O, which requires higher temperatures. Thus, the true (F = 0) solidus temperature of carbonated peridotite likely varies less than the solidus that we detected experimentally, which likely corresponds to magnesite-out. As pointed out above, however, both solidi converge to the same temperature at very low bulk CO_2 concentrations.

Control of $CaCO_3$-$MgCO_3$ binary on the natural carbonated peridotite solidus

Because the dominant near-solidus melting reaction in carbonated peridotite involves reaction between Ca-bearing Mst_{ss} and Ca, Mg-rich carbonatite liquid, the melting relations are in part analogous to the topology of the $MgCO_3$-$CaCO_3$ phase diagram (Irving and Wyllie 1975; Buob et al. 2006). In experiments at 6 GPa, Buob et al. (2006) found a minimum melting temperature for Mst_{ss} of 1340 °C. Extrapolation of these results, guided by lower pressure experiments (Irving and Wyllie 1975; Byrnes and Wyllie 1981) suggests that this minimum increases to ~1400 °C at 6.6 GPa. This value closely matches the ~1415 °C melting temperature at 6.6 GPa for model CMAS-CO_2 peridotite (interpolated from solidus of 1380 °C at 6 and 1430 °C at 7 GPa; Dalton and Presnall 1998). The similarity between the minimum melting temperature at 6 GPa for CM-CO_2 (Buob et al. 2006) and that of the solidus temperature for peridotitic CMAS-CO_2 system (Dalton and Presnall 1998) led Buob et al. (2006) to conclude that, at pressures ≥3 GPa, the location of the solidus minimum in the $CaCO_3$-$MgCO_3$ binary has a principal influence on the temperature, phase relations, and melt compositions of near-solidus melting of complex carbonated silicate systems such as CMAS-CO_2 and of low-alkali natural carbonated peridotite and eclogite. In contrast, the present study clearly demonstrates that the solidi of natural carbonated peridotites are 100 to 200 °C lower than the minima of the $CaCO_3$-$MgCO_3$ binary or the peridotite solidus in CMAS-CO_2. The difference is related to the fluxing effects of FeO* and Na_2O.

If we consider only FeO* and alkali-free peridotite compositions (e.g., CMAS-CO_2, Dalton and Presnall 1998), then solidus temperatures are similar to the CM-CO_2 solidus minimum, because the temperature of the solidus for the latter varies by less than 50 °C over a wide range of Ca no., from 0.10 to 0.50 (Fig. 4). However, the phase relations of solidus melting at the CM-CO_2 minimum are distinct from the CMAS-CO_2 peridotite solidus. The former requires that crystalline carbonate have a Ca no. of ~0.50 ± 0.10 (at 6 GPa), whereas silicate-carbonate equilibria in synthetic peridotite requires near-solidus carbonates with a Ca no. of 0.05 ± 0.05 and in this compositional

range, modest variations in solid carbonate Ca no. can have significant influence on the solidus temperature.

Melting reactions of natural magnesite-lherzolite

Use of the estimated phase proportions from Table 2 and the method of Walter et al. (1995) yields the following approximate melting reactions for magnesite lherzolite at 6.6 GPa:

$$3\ \text{cpx} + 2\ \text{gt} + 2\ \text{mst} = 4\ \text{opx} + 3\ \textit{cbl}\ \text{(PERC3)} \quad (2)$$

$$6\ \text{cpx} + 5\ \text{mst} + 1\ \text{ol} + 1\ \text{gt} = 7\ \text{opx} + 6\ \textit{cbl}\ \text{(PERC)} \quad (3)$$

$$14\ \text{cpx} + 10\ \text{mst} + 1\ \text{gt} = 14\ \text{opx} + 11\ \textit{cbl}\ \text{(PERC2)} \quad (4)$$

The exact values of coefficients for bulk compositions PERC and PERC3 remain somewhat uncertain, as there is only one analysis of a melt pool in each; however, the estimates for carbonatite melt fraction produced for each reaction are consistent with those expected from the proportion of added carbonate, taking into account that the melts contain ~40 wt% CO_2. These melting reactions suggest that the dominant melting reaction at the solidus of magnesite-lherzolite is

$$\underset{\text{mst}}{2MgCO_3} + \underset{\text{cpx}}{CaMgSi_2O_6} = \underset{\text{cbl}}{CaMg(CO_3)_2} + \underset{\text{opx}}{Mg_2Si_2O_6}. \quad (5)$$

The melting reactions 2–4 are similar to those found at 6–7 GPa for CMAS-CO_2 magnesite-lherzolite (Dalton and Presnall 1998), but in the latter case, excess CO_2 in the bulk starting material produces more Mst_{ss} in the subsolidus assemblage, which in turn produces more carbonate melt and consumes a larger proportion of cpx (Fig. 3b).

Solidus of natural carbonated peridotite

Understanding the effect of bulk composition on experimental near-solidus melting of carbonated peridotite allows consideration of the likely partial melting behavior of natural carbonated peridotite. Assuming peridotite in basalt source regions with a major-element composition similar to MixKLB-1 (Table 1), the solidus at 6.6 GPa can be found by linear extrapolation of solidus temperatures vs. bulk CO_2 contents down to concentrations appropriate for mid-ocean ridge basalt (MORB) sources (50–1000 ppm CO_2) (Saal et al. 2002) or oceanic island basalt (OIB) sources (1000–4000 ppm CO_2) (Trull et al. 1993; Dixon et al. 1997; Pineau et al. 2004). For a MORB source, the solidus is ~1200 ± 20 °C and for OIB it can be 10–20 °C higher.

At 6.6 GPa, the solidus for peridotite with small amounts (10 to 1000s of ppm CO_2) is ca. 600 degrees lower than the volatile-free peridotite at 6.6 GPa (~1785 °C) (Hirschmann 2000). This solidus should prevail as long as trace quantities of a carbonate mineral (i.e., magnesite) are present at the solidus. If carbon is stored in reduced form, as graphite or diamond, then the solidus will be controlled by redox melting reactions that occur at slightly higher temperatures than pure carbonated melting reactions (Wood et al. 1996; Luth 2003; Dasgupta and Hirschmann 2006). Alternatively, if concentrations are very low, C may be incorporated entirely as a trace point defect in nominally C-free silicates. Experiments by Keppler et al. (2003) indicate a peridotite with 60% olivine, 10% opx, 15% cpx, and 15% garnet may plausibly dissolve not more than 5 ppm CO_2. For these very low C concentrations, the solidus will not be appreciably different from the C-free case (Fig. 7).

Compositions of mantle peridotites vary, including in Ca no., Mg no., and alkali contents. Although further investigations of these compositional variables are desirable, it is likely that their effects are strongly attenuated for total CO_2 concentrations similar to those found in nature (100s to 1000 of ppm). This is perhaps best illustrated by Figure 6, which demonstrates that (1) variations in Na_2O/CO_2 have greater influence than Ca no. or Mg no.; and (2) changes in solidus owing to Na_2O/CO_2 variations diminish when Na_2O/CO_2 is large, as argued above. An important caveat to this discussion, however, is that the effects of H_2O and K_2O on the solidus of carbonated peridotite are poorly constrained.

Comparison with the effect of H_2O on the peridotite solidus

Small variations in the solidus temperature of carbonated peridotite with increases in bulk CO_2 contrasts with the influence of H_2O. For the latter, increases in H_2O concentration result in decreases in melting temperature (except at high H_2O concentrations, where fluid saturation occurs). The distinct effects of CO_2 and H_2O can be understood from their differences in storage in solids and in the composition of the resulting melts. H_2O is stored in nominally anhydrous minerals (NAMs) (Bell and Rossman 1992), with variable bulk concentrations resulting in variable activities of H_2O. Near-solidus partial melt stabilized by CO_2 is carbonatitic, so CO_2 concentrations do not vary appreciably, whereas near-solidus partial melt stabilized by H_2O is a hydrous silicate, in which H_2O concentrations change according to the activity of H_2O imposed by coexisting minerals. Thus, solidus temperatures should decrease significantly with increasing concentrations of H_2O, but the effects of variable concentrations of CO_2 are more subtle.

The different effects of H_2O and CO_2 on peridotite solidi are illustrated in Figure 7. Whereas nominally volatile-free silicates can sequester just a few ppm CO_2 (Keppler et al. 2003), at high pressure they may store several thousand ppm H_2O (Kohlstedt et al. 1996; Hirschmann et al. 2005). With increasing H_2O stored in nominally anhydrous silicates, the solidus temperature of peridotite diminishes continuously (Hirth and Kohlstedt 1996; Katz et al. 2003; Asimow et al. 2004; Aubaud et al. 2004). Owing to greater H_2O concentrations in OIB source regions, the solidus depression owing to H_2O will be greater than beneath ridges. Once saturation with an H_2O-rich fluid is attained, the solidus is nearly constant (Kawamoto and Holloway 1997), although small increases or decreases owing to changing fluid compositions are feasible. Thus, as shown in Figure 7, the solidus of peridotite diminishes continuously with increasing H_2O until fluid saturation is reached. In contrast, the solidus diminishes suddenly as soon as carbonate saturation is reached at very low concentration, and then is little-affected by variable concentrations of CO_2 until wt% levels are achieved, similar to those employed in the present experiments, at which point the solidus apparently increases.

Concluding remarks

• Experimentally determined solidi of natural carbonated peridotite at 3–6.6 GPa are 100 –200 °C lower than those of CMAS-CO_2 peridotite, chiefly owing to the fluxing effect of alkalis. The solidus of natural carbonated peridotite is ~450–600 °C lower than the solidus of natural volatile-free solidus from 3 to 6.6 GPa.

• At 6.6 GPa, the experimental solidus of magnesite lherzolite decreases with increasing bulk Na_2O/CO_2, owing to increasing Na_2O in near-solidus carbonate melt. Consequently, the solidus of fertile peridotite + CO_2 with small amounts (hundreds or thousands of ppm) of CO_2 is ~1200 ±25 °C, ~20–100 °C lower than that determined directly from experiments that employ 1–5 wt% CO_2.

• The effects of bulk composition on solidi of peridotite are likely magnified by experiments with approximate percent concentrations of CO_2. Variations in bulk composition likely have much smaller effect when CO_2 is present in natural (hundreds–thousands ppm) concentrations.

• With increasing bulk CO_2, the solidus of peridotite will drop discontinuously at about ~5 ppm, where crystalline carbonate is first stabilized. Below ~5 ppm CO_2, the solidus is similar to that of volatile-free peridotite, but above this threshold, it is ~600 °C lower (at 6.6 GPa). Further increases in bulk CO_2 induce negligible increases in the solidus (though they do increase the proportion of melt generated near the solidus). This contrasts with the effect of H_2O, which diminishes the solidus with increasing addition to peridotite.

ACKNOWLEDGMENTS

We are grateful for the constructive reviews from Max Schmidt and Chip Lesher. R.D. acknowledges support from the Graduate School of University of Minnesota through a Doctoral Dissertation Fellowship. This work also received support from National Science Foundation grant EAR 0310142 to M.M.H.

REFERENCES CITED

Asimow, P.D., Dixon, J.E., and Langmuir, C.H. (2004) A hydrous melting and fractionation model for mid-ocean ridge basalts: Application to the Mid-Atlantic Ridge near the Azores. Geochemistry Geophysics Geosystems, 5, Q01E16, DOI: 10.1029/2003GC000568.

Aubaud, C., Hauri, E.H., and Hirschmann, M.M. (2004) Hydrogen partition coefficients between nominally anhydrous minerals and basaltic melts. Geophysical Research Letters, 31, L20611, DOI: 10.1029/2004GL021341.

Bell, D.R. and Rossman, G.R. (1992) Water in Earth's Mantle: the role of nominally anhydrous minerals. Science, 255, 1391–1397.

Buob, A., Luth, R.W., Schmidt, M.W., and Ulmer, P. (2006) Experiments on $CaCO_3$-$MgCO_3$ solid solutions at high pressure and temperature. American Mineralogist, 91, 435–440.

Byrnes, A.P. and Wyllie, P.J. (1981) Subsolidus and melting relations for the join $CaCO_3$-$MgCO_3$ at 10 kbars. Geochimica et Cosmochimica Acta, 45, 321–328.

Canil, D. (1990) Experimental study bearing on the absence of carbonate in the mantle-derived xenoliths. Geology, 18, 1011–1013.

Canil, D. and Scarfe, C.M. (1990) Phase relations in peridotite + CO_2 systems to 12 GPa: implications for the origin of kimberlite and carbonate stability in the Earth's upper mantle. Journal of Geophysical Research, 95, 15805–15816.

Dalton, J.A. and Presnall, D.C. (1998) Carbonatitic melts along the solidus of model lherzolite in the system CaO-MgO-Al_2O_3-SiO_2-CO_2 from 3 to 7 GPa. Contribution to Mineralogy and Petrology, 131, 123–135.

Dasgupta, R. (2006) Experimenal investigation of mantle melting in the presence of carbonates, p. 247. Ph.D. thesis, University of Minnesota, Minneapolis.

Dasgupta, R. and Hirschmann, M.M. (2006) Melting in the Earth's deep upper mantle caused by carbon dioxide. Nature, 440, 659–662.

Dasgupta, R., Hirschmann, M.M., and Withers, A.C. (2004) Deep global cycling of carbon constrained by the solidus of anhydrous, carbonated eclogite under upper mantle conditions. Earth and Planetary Science Letters, 227, 73–85.

Dasgupta, R., Hirschmann, M.M., and Dellas, N. (2005) The effect of bulk composition on the solidus of carbonated eclogite from partial melting experiments at 3 GPa. Contributions to Mineralogy and Petrology, 149, 288–305.

Dixon, J.E., Clague, D.A., Wallace, P., and Poreda, R. (1997) Volatiles in alkalic basalts from the north arch volcanic field, Hawaii: extensive degassing of deep submarine-erupted alkalic series lavas. Journal of Petrology, 38, 911–939.

Falloon, T.J. and Green, D.H. (1989) The solidus of carbonated, fertile peridotite. Earth and Planetary Science Letters, 94, 364–370.

Galer, S.J.G. and O'Nions, R.K. (1986) Magmagenesis and the mapping of chemical and isotopic variations in the mantle. Chemical Geology, 56, 45–61.

Herzberg, C., Feigenson, M., Skuba, C., and Ohtani, E. (1988) Majorite fractionation recorded in the geochemistry of peridotites from South Africa. Nature, 332, 823–826.

Hirschmann, M.M. (2000) The mantle solidus: experimental constraints and the effect of peridotite composition. Geochemistry Geophysics Geosystems, 1, 2000GC000070.

Hirschmann, M.M., Asimow, P.D., Ghiorso, M.S., and Stolper, E.M. (1999) Calculation of peridotite partial melting from thermodynamic models of minerals and melts. III. Controls on isobaric melt production and the effect of water on melt production. Journal of Petrology, 40, 831–851.

Hirschmann, M.M., Aubaud, C., and Withers, A.C. (2005) Storage capacity of H_2O in nominally anhydrous minerals in the upper mantle. Earth and Planetary Science Letters, 236, 167–181.

Hirth, G. and Kohlstedt, D.L. (1996) Water in the oceanic upper mantle: implications for rheology, melt extraction and the evolution of the lithosphere. Earth and Planetary Science Letters, 144, 93–108.

Holloway, J.R. and Blank, J.G. (1994) Application of experimental results to C-O-H species in natural melts. In M.R. Carroll and J.R. Holloway, Eds., Volatiles in Magmas, 30, p. 186–230. Reviews in Mineralogy, Mineralogical Society of America, Chantilly, Virginia.

Irving, A.J. and Wyllie, P.J. (1975) Subsolidus and melting relationships for calcite, magnesite and the join $CaCO_3$-$MgCO_3$ to 36 kb. Geochimica et Cosmochimica Acta, 39, 35–53.

Jambon, A. (1994) Earth degassing and large-scale geochemical cycling of volatile elements. In M.R. Carroll and J.R. Holloway, Eds., Volatiles in Magmas, 30, p. 479–517. Reviews in Mineralogy, Mineralogical Society of America, Chantilly, Virginia.

Katz, R.F., Spiegelman, M., and Langmuir, C.H. (2003) A new parameterization of hydrous mantle melting. Geochemistry Geophysics Geosystems, 4, 1073, DOI: 10.1029/2002GC000433.

Kawamoto, T. and Holloway, J.R. (1997) Melting temperature and partial melt chemistry of H_2O-saturated mantle peridotite to 11 Gigapascals. Science, 276, 240–243.

Keppler, H., Wiedenbeck, M., and Shcheka, S.S. (2003) Carbon solubility in olivine and the mode of carbon storage in the Earth's mantle. Nature, 424, 414–416.

Kohlstedt, D.L., Keppler, H., and Rubie, D.C. (1996) Solubility of water in the α, β and γ phases of $(Mg,Fe)_2SiO_4$. Contributions to Mineralogy and Petrology, 123, 345–357.

Luth, R.W. (1993) Diamonds, eclogites, and oxidation state of the Earth's mantle. Science, 261, 66–68.

——— (1999) Carbon and carbonates in the mantle. In Y. Fei, C.M. Bertka, and B.O. Mysen, Ed., Mantle Petrology: Field Observations and High Pressure Experimentation: A Tribute to Francis R. (Joe) Boyd, 6, p. 297–316. The Geochemical Society, Houston, Texas.

——— (2003) Mantle volatiles—distribution and consequences. In R.W. Carlson, Ed., The mantle and core, 2, p. 319–361. Elsevier, Amsterdam.

Olafsson, M. and Eggler, D.H. (1983) Phase relations of amphibole, amphibole-carbonate, and phlogopite-carbonate peridotite: petrologic constraints on the asthenosphere. Earth and Planetary Science Letters, 64, 305–315.

Pineau, F., Shilobreeva, S., Hekinian, R., Bidiau, D., and Javoy, M. (2004) Deep-sea explosive activity on the Mid-Atlantic Ridge near 34° 50' N: a stable isotope (C, H, O) study. Chemical Geology, 118, 43–64.

Plank, T. and Langmuir, C.H. (1992) Effects of melting regime on the composition of the oceanic crust. Journal of Geophysical Research, 97, 19749–19770.

Presnall, D.C., Gudfinnsson, G.H., and Walter, M.J. (2002) Generation of mid-ocean ridge basalts at pressures from 1 to 7 GPa. Geochimica et Cosmochimica Acta, 66(12), 2073–2090.

Saal, A.E., Hauri, E., Langmuir, C.H., and Perfit, M.R. (2002) Vapour undersaturation in primitive mid-ocean-ridge basalt and the volatile content of Earth's upper mantle. Nature, 419, 451–455.

Trull, T., Nadeau, S., Pineau, F., Polve, M., and Javoy, M. (1993) C-He systematics in hotspot xenoliths: implications for mantle carbon contents and carbon recycling. Earth and Planetary Science Letters, 118, 43–64.

Wallace, M.E. and Green, D.H. (1988) An experimental determination of primary carbonatite magma composition. Nature, 335, 343–346.

Walter, M.J., Sisson, T.W., and Presnall, D.C. (1995) A mass proportion method for calculating melting reactions and application to melting of model upper mantle lherzolite. Earth and Planetary Science Letters, 135, 77–90.

Wendlandt, R.F. and Mysen, B.O. (1980) Melting phase relations of natural peridotite + CO_2 as a function of degree of partial melting at 15 and 30 kbar. American Mineralogist, 65, 37–44.

Wood, B.J., Pawley, A., and Frost, D.R. (1996) Water and carbon in the Earth's mantle. Philosophical Transaction Royal Society London, 354, 1495–1511.

Wyllie, P.J. and Huang, W.-L. (1975) Influence of mantle CO_2 in the generation of carbonatites and kimberlites. Nature, 257, 297–299.

Yaxley, G.M. and Green, D.H. (1996) Experimental reconstruction of sodic dolomitic carbonatite melts from metasomatised lithosphere. Contributions to Mineralogy and Petrology, 124, 359–369.

MANUSCRIPT RECEIVED DECEMBER 27, 2005
MANUSCRIPT ACCEPTED SEPTEMBER 19, 2006
MANUSCRIPT HANDLED BY PAUL ASIMOW